POLITECNICO DI TORINO
Repository ISTITUZIONALE

The Buoyancy of the Tunnel Segmental Lining in the Surrounding Filling Material and its Effects on the Concrete Stress State

Original
The Buoyancy of the Tunnel Segmental Lining in the Surrounding Filling Material and its Effects on the Concrete Stress State / Han, X., Oreste, P., Ye, F.. - In: GEOTECHNICAL AND GEOLOGICAL ENGINEERING. - ISSN 0960-3182. - 41:2(2023), pp. 741-758. [10.1007/s10706-022-02299-z]

Availability:
This version is available at: 11583/2980295 since: 2023-07-13T19:13:28Z

Publisher:
Springer Science and Business Media Deutschland GmbH

Published
DOI:10.1007/s10706-022-02299-z

Terms of use:

This article is made available under terms and conditions as specified in the corresponding bibliographic description in the repository

Publisher copyright

(Article begins on next page)

01 November 2026

Geotech Geol Eng (2023) 41:741–758
https://doi.org/10.1007/s10706-022-02299-z

ORIGINAL PAPER

The Buoyancy of the Tunnel Segmental Lining in the Surrounding Filling Material and its Effects on the Concrete Stress State

Xin Han · Pierpaolo Oreste · Fei Ye

Received: 23 July 2022 / Accepted: 7 September 2022 / Published online: 10 October 2022
© The Author(s) 2022

Abstract Segmental lining is subject to significant upward buoyancy forces when a grouting material (slurry), initially fluid, is adopted to fill the gap between its external profile and the wall of a tunnel excavated with a TBM machine. The analysis of the effects of these forces is important in order to correctly dimension the segmental lining and avoid damage to the lining and subsequent costly maintenance and restoration actions. Given the complexity of the behavior of a segmental lining consisting of segmental rings and circular joints that alternate in the longitudinal direction of the tunnel, a specific numerical model has been implemented, adopting the Finite Element Method (FEM). This model is able to obtain the development of the vertical displacements of the segmental lining starting from the TBM tail, together with the bending moments and the shear forces induced inside it. The developed model is able to assess the risks of breaking and damaging the concrete and steel bolts that are used to connect the segmental rings at the circular joints; therefore, it represents a useful design tool for being able to correctly dimension the segmental lining also in relation to the risks produced by the appearance of considerable buoyancy forces around it, due to the presence of the initially fluid filling material. The proposed numerical model was applied to a real case (Ningbo metro tunnel) and allowed to obtain satisfactory results from the comparison of the calculated displacements with in situ measurements. Some sensitivity analyzes developed on the studied case have made it possible to detect which are the influencing parameters that have the greatest impact on the behavior of segmental lining in the presence of the studied buoyancy forces.

Keywords Shield tunnels · Segmental lining · Buoyancy phenomenon · Finite element method (FEM) · Lining deformation · Joint behaviour

1 Introduction

Due to the advantages of undisturbed urbanised surface, cost-effectiveness of excavation, low settlement risks of the structures surrounding the tunnel, improved safety conditions, Tunnel Boring Machines (TBMs) has been widely used in the last decades to construct tunnels in the metro, highway and railway systems (Dastjerdy et al. 2018; Innaurato et al. 2011). The use of TBMs generally requires the insertion of a particular type of tunnel support structure: the segmental lining (Fig. 1) (Do et al. 2013, 2014, 2015; Zaheri et al. 2020).

X. Han · F. Ye
School of Highway, Chang'an University, Middle-section of Nan'er Huan Road, Xi'an, ShaanXi 710064, PR China

X. Han · P. Oreste (✉)
Department of Environmental, Land and Infrastructure Engineering (DIATI), Politecnico di Torino, Corso Duca degli Abruzzi 24, 10129 Turin, Italy
e-mail: pierpaolo.oreste@polito.it

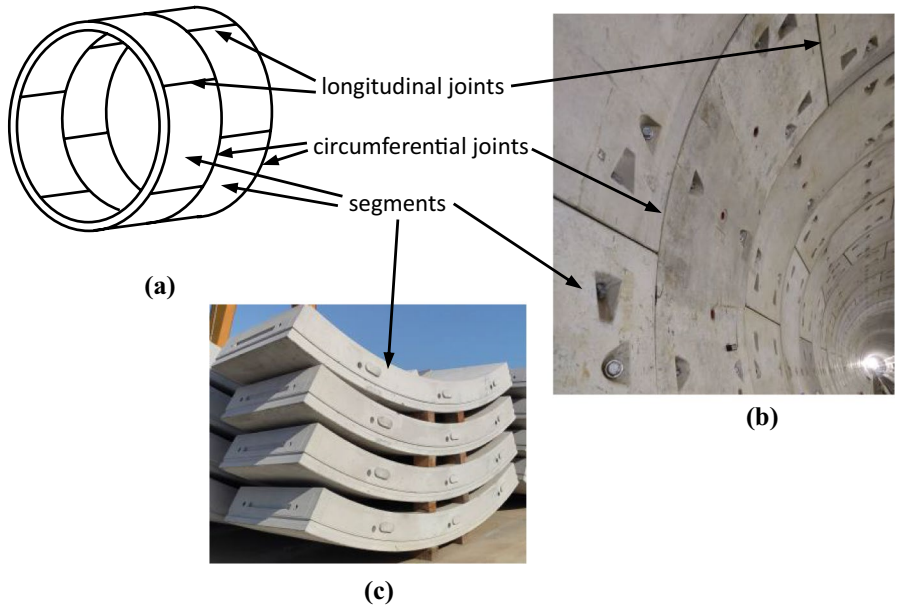


Fig. 1 Segmental lining of a tunnel. Key: **a** isometric view, **b** inner view of a completed tunnel, **c** segments stacked in the construction site before their insertion inside the tunnel

However, the occurrence frequency of cracking, leakage and dislocation phenomenon of segment linings is increasing during the construction stage (Han et al. 2017): corner cracks and longitudinal cracks are the main types of damage of the concrete segmental lining (Xu et al. 2019). The overall stiffness and the plastic bearing range of the structures will be reduced with the appearance and extension of cracks (Wang et al. 2020).

The main reasons of cracks formation in segments are concluded by Wu (2004). Apart from the production and the transportation and the segment quality (15.2%), the other factors are determined by the excavation progress during the construction period, which includes the assembling quality of the segment itself, the jacking forces, the synchronous grouting pressure, and the attitude deviation between shield machine and segments. Ye et al. (2020) also indicate the three main construction actions that frequently produced longitudinal cracks, including the invasion of shield tail at small curvature radius tunnel, the jack thrusting of large shield tunnel, the unsymmetrical pressure from the backfill grouting pressure. Compared with the loads acting on the tunnel lining at the service period, the loads and the constraints during the construction period are more complex and variable along the longitudinal direction of the tunnel and are applied by the jack system, shield tail wire brush, slurry and ground (Fig. 2).

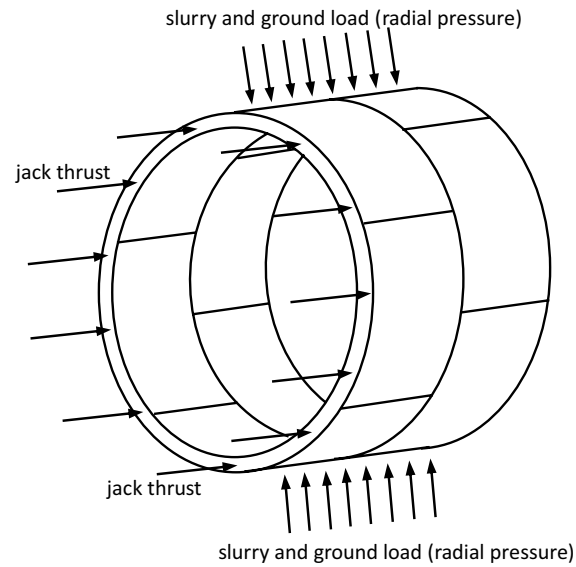


Fig. 2 Main loads applied to the segmental lining during the construction stage

In order to more precisely understand the damage process of segmental lining during construction, the deformation and the stress state of the segmental lining along the longitudinal direction need to be analysed. With the application of external loads on the tunnel lining, an uneven displacement is detected along the longitudinal direction and it will cause opening

of circumferential joints, dislocation of the adjacent segment rings and damage of segment lining (Huang et al. 2012; Liu et al. 2021a, c; Wang et al. 2014). So, when solving the lining deformation problem, the first key point is to find a model which can represent the structural performance. Especially, it could express the stiffness of the segmental lining before and after any deformation, because the segmental lining is connected by the steel bolts along the circumferential and the longitudinal direction, and the stiffness of the joints is affected by the contact pattern. The uneven displacement is more common during the shield tunnel construction, which was led by the restraint forces from the shield shell, liquid slurry in the gap between the tunnel wall and the outer border of the lining and different ground strata surrounding the tunnel (Talmon and Bezuijen 2013). The determination of the loads on the lining during the construction is another key point.

In the analysis of the longitudinal deformation of a tunnel segmental lining, the circular joint behaviour is critical (Cheng et al. 2021, 2020; Li et al. 2019; Liao et al. 2008; Liu et al. 2021a; Wu et al. 2015, 2018). Based on the beam theory, Shiba et al. (1988) simplified the segmental lining as a continuous beam with a reduced stiffness due to the presence of joints, but the influence of the segments and the joints separately on the damage of the segmental lining cannot be discussed using these simplified methods. Koizumi et al. (1988) proposed the beam-spring model to study the segmental lining along the longitudinal direction; they simulated concrete annuli and circumferential joints using short beams and three dimensions springs elements respectively. However, the computational complexity of the model and the difficulty in determining the spring stiffnesses restricted the application of this model (Wu et al. 2015). In order to evaluate longitudinal differential deformations and stress states inside concrete segments, a 3D discontinuous contact model was built considering both the circumferential contact and longitudinal contact (Arnau and Molins 2012; Chaipanna and Jongpradist 2019; Liu et al. 2021b, c). However, the 3D model has a very complex initial configuration and also is time-consuming during the calculation and for these reasons is not friendly for a quick evaluation in the engineering design stage. Therefore, developing a new model which can represent the effect of the individual joint, and can be resolved quickly is necessary and useful for the analysis of the lining deformation (Peila et al. 1995; Spagnoli et al. 2016).

Accompanying the excavation by the cutting head, the segments are fixed and connected by bolts under the protection of the shield shell, and come out of the shield tail with the TBM advancement. Due to the gap of the diameter between the cutting wheel and the precast concrete segments, there is always an annular gap around the lining, which can be filled with a synchronous grouting material (Wang et al. 2019) (the traditional solution). Based on requirements of the long-distance transportation and the alternative process of TBM advancement and segment assembly, a high flowability, stability and pumpability and the fast development of strengths need to be fulfilled by the filling material (slurry) (Youn and Breitenbücher 2014). However, the desired workability before grouting and the strength development after grouting are contradictory requirements for a slurry (Youn and Breitenbücher 2018). The two-component slurry is used in order to obtain a fast development of the strength and stiffness; the material A, which is composed of cement, bentonite, fly ash, et. al, is mixed with the material B, which is composed of an accelerator admixture (sodium silicate and water) (Todaro et al. 2020). However, there is a high requirement for technology and equipment in the two-component slurry compared with the traditional grouting, due to the mixing procedure inside the grouting hole. Nowadays about 80% of TBM tunnels in China (a preliminary estimation based on a synthetic survey) uses the single-component grouting mortars as the synchronous grouting material (Liang et al. 2022), in order to assure a lower risk of grouting pipe blockage, lower requirements of equipment and also to avoid operation difficulties. Because the increase of the setting time of the filling material and the speed of the TBM machine lead to an increase of the length of the liquid slurry, which further increase the uplift risk of the tunnel lining (Peila et al. 2011); finding the relationship between the applied loads by the slurry on the segmental lining and the main influencing parameters is important to analyse and control the segmental lining damage.

In the still liquid portion of slurry, near the TBM tail, the segmental lining is subject to some huge forces directed upwards due to the buoyancy effect. These additional applied forces produce bending moments and shear forces along the longitudinal direction of the segmental lining; this state of stress is added to the stresses produced by the radial pressure applied by the slurry and by the ground surrounding

the segmental lining. Therefore, to assess the risk of damage to the segmental lining during the construction phase of the tunnel, the buoyancy effect and the development of bending moments and shear forces along the longitudinal direction of the segmental lining cannot be neglected.

A specific numerical approach to the upward uneven displacement of the tunnel lining along its axis and during construction, due to the buoyancy effect, is presented in this paper. The proposed approach is able to evaluate the risk of damage of the segmental lining on the basis of a specific developed Finite Element Method (FEM) model (Pelizza et al. 2000). The model is able to quickly determine the trend of bending moments and shear forces, as well as vertical displacements, along the axis of the tunnel starting from the initial zone of the segmental lining, close to the TBM tail. Thanks to the evaluation of the induced stresses, it is then possible, from the comparison with the concrete strength values, to determine the safety factors with regard to the possible damage and to understand the level of risk that the segmental lining may be exposed during the construction of the tunnel.

2 The Buoyancy Effect of the Segmental Lining Inside the Liquid Slurry (Grout) Close to the TBM Tail

2.1 The Evolution of the Physical and Mechanical Characteristics of the Slurry Versus Time (Hardening Time)

Due to the hydration process, mechanical characteristics of the slurry will change over time and the restraint of the lining by the slurry has an uneven intensity (Chen et al. 2018). Due to the wide use of slurry, the parameters used to describe its physical and mechanical characteristics are available in the scientific literature. The parameters can be divided into two types: (1) fluidity, hardening time, bleeding rate and viscosity for fluid slurry; (2) compressive strength, flexural strength, shear strength, bulk shrinkage rate, scour resistance and durability for solid slurry (He et al. 2020; Liang et al. 2022; Mao et al. 2020). The hardening time and the strength are the main characteristics of a slurry. The composition of the slurry has a great influence on its characteristics (Mao et al. 2020), such as the accelerator admixture shortening the hardening time (Todaro et al. 2020). Some tunnel construction cases were collected and the main slurry parameters are listed in Table 1.

From Table 1 it is possible to see how a slurry consistency of about 8–12 cm and a bleeding rate less than 5% are generally required. The hardening time is about 3–18 h based on the geological of surrounding ground and considering the transportation and the diffusion process of slurry; many projects require a hardening time of less than 10 h. The slurry compressive strength is about 0.1 MPa on the 1st day, about 0.38 MPa on the 7th day, and about the strength of the surrounding ground on the 28th day.

In order to control the hardening time and strength, the effects of composition of slurry on its characteristic was also studied. Some results are shown in Table 2.

According to Table 2, the hardening time is about 3–15 h, and the strength is about 1 MPa on the 3rd day from slurry mixing, and about 5 MPa on the 28th day, based on indoor tests.

Table 1 Main slurry parameters for some tunnel construction cases known in the scientific literature

Consistency (cm)	Bleeding rate (%)	Hardening time (h)	Compressive strength (MPa)		Shield tunnel case	Reference
/	≤5	12–18	/	> 2(28d)	South-to-North Water Transfer Project	Liang (2006)
8–12	< 5	3–10	≥ 0.15(1d)	≥ 1.5(28d)	/	Liang (2009)
8	≤14	6–10	> 0.38(7d)	> 1.65(28d)	Suzhou metro Line 2	Yu (2011)
8–12	< 5	/	≥ 0.2(1d)	≥ 2.5(28d)	Diversion tunnel	You et al. (2012)
9–11	/	3–10	≥ 0.1(1d)	> 2.5(28d)	Nanchang metro Line 4	Dong et al. (2021)

The parameters are tested on the basis of the Chinese Standard (China 2009)

Table 2 Physical and mechanical characteristics of the slurry, varying its composition

Composition of the slurry (kg/m^3)						Hardening time (h)	Strength (MPa)		Specific mass (kg/m^3)	Reference
C	F	S	B	W	A		3 d	28 d		
91	365	920	20	320	0	/	0.9	5.3	1875	Tian (2007)
91	365	920	0	320	4.56 (1)	/	0.8	4.3	1862	Tian (2007)
125	275	780	60	365	0	/	1.2	5.2	1723	Tian (2007)
160	270	900	70	400	2.65 (2)	3.6	/	5.2	1750	You et al. (2012)
160	270	900	70	400	3.44 (2)	4.5	/	6.3	1760	You et al. (2012)
150	352	837	52	433	0	5.0	/	3.75	/	Liang (2009)
240	352	837	52	309	0	3.6	/	10.1	/	Liang (2009)
187	313	770	37.5	375	4.25	15.0	/	/	/	Liang (2006)
200	300	1000	45	300	2.5	5.0	/	/	/	Liang (2006)

C cement, *F* Fly ash, *S* sand, *B* bentonite, *W* water, *A* admixture, *(1)* HBP-5, *(2)* HT-HPC

2.2 The Buoyancy Effect of the Segmental Lining in the Fluid Zone of the Slurry Close to the TBM Tail

In general, the segmental lining is wrapped and loaded by the slurry and the surrounding ground. Based on the Archimedes' principle, the buoyant force (an upward vertical force per meter along the longitudinal direction of the tunnel), q_{buo}, is equal to the weight of the liquid replaced by the body, and can be calculated by the surface integral approach. A simply method is the pressure gradient:

$$q_{buo} = g \cdot \pi \cdot R^2 \tag{1}$$

where g is the vertical pressure gradient of the slurry, R is the external radius of the segmental lining.

During the construction of the Sophia Rail Tunnel, Bezuijen et al. (2004) measured the vertical pressure gradient and found that it was less than the volumetric weight. The researchers gave three reasons for this difference: firstly, the downward flow of slurry will lead to a pressure decrease to maintain the flow; secondly, the measured gradient is influenced by the moments of the lining which is connected to the TBM and to adjacent segment rings; thirdly, the rheological properties of slurry also influence the measured values, and the dewatering will improve the yield stress. For these reasons it is difficult to obtain accurate buoyant force values by field testing.

Based on the Fluid Mechanics (White 2011), the buoyant force can be simply estimated by the specific weight of the slurry and the volume of the segment lining (Eq. 1), where the vertical pressure gradient of the slurry, g, is equal to the specific weight of the slurry, γ_{sl}. Due to the slurry viscosity (that is low at the initial stage) and the very slow displacement velocity of the segment lining, the resistance can be neglected and the buoyant force is the main lateral load applied to the segment lining. So, regarding the initial stage of slurry, the vertical load on the segment lining,q, can be obtained under the influence of segmental gravity:

$$q = \gamma_{sl} \cdot \frac{\pi}{4} \cdot D^2 - \gamma_{con} \cdot \frac{\pi}{4} \cdot \left[D^2 - (D - 2t)^2\right] \tag{2}$$

where γ_{con} is the specific weight of concrete, D and t are the external diameter of the lining and its thickness, respectively.

However, with the increase of time, the viscosity of the slurry (when it is fluid) and strength (when solid) also increases gradually (Mahmoodzadeh and Chidiac 2013). Due to the considerable resistance toward the segment's movement of the hardening slurry together to the surrounding ground, the longitudinal vertical section can be divided into two zones: the fluid slurry zone and the solid slurry one (Fig. 3). The presence of the solid slurry can be represented by vertical springs (Winkler springs) able to react to the upward movement of the segmental lining (the segmental gravity and the pressure due to the self-weight of slurry and ground are neglected). Winkler springs are often adopted in order to simulate the interaction between the soil/rock mass and a support/reinforcing structure (Oreste 2013). Because of the upward movement of the segmental lining in the fluid slurry zone and the gradual hardening of the slurry, the initial position of segments at the beginning of the solid slurry zone is

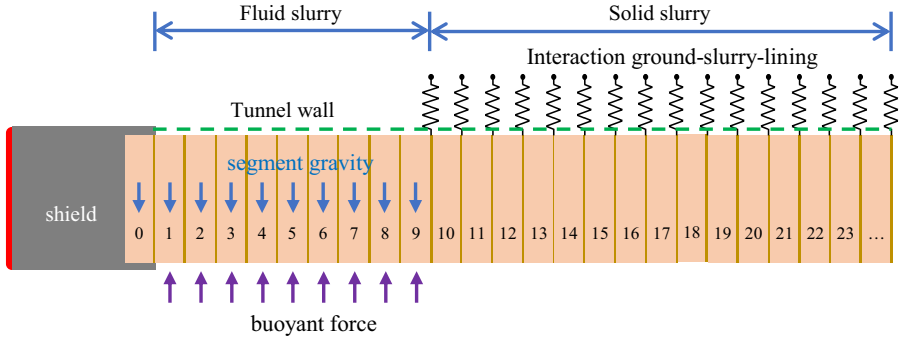


Fig. 3 Vertical longitudinal section of the segmental lining close to the TBM tail. In the fluid slurry zone buoyant forces are applied to the segmental lining; in the solid slurry zone, Winkler springs simulate the reaction of the slurry and the surrounding ground to the movement of the segmental lining

assumed to be equal to the vertical displacement of the final segment of the fluid slurry zone.

2.3 The Fluid Slurry Zone and the Boundary Conditions of the Lining

The length of the fluid slurry zone is influenced by the average speed of the TBM machine and by the hardening evolution of the slurry. The speed of the TBM machine can be calculated by the total time required to complete a ring, including the excavation time and the segment assembling time. The hardening time of the slurry can describe the transformation from fluid to solid: the specific test JGJ/T 70-2009 (China 2009) with the penetration resistance method permits to define the hardening time as the time related to a value of the penetration resistance of 0.5 MPa. Then, the length d of the fluid slurry zone can be obtained by:

$$d = v \cdot t_0 \tag{3}$$

where v is the gross average speed of the TBM machine, t_0 is the hardening time of the slurry.

The first segment is inside the shield, and is constrained by the shield tail brush: no displacements neither rotations can be admitted to this extreme of the lining. No other types of constraints are present along the lining in the longitudinal direction.

3 A Specific FEM Numerical Model to Study the Effect of Buoyancy Forces on the Segmental Lining

The longitudinal representation of the segmental lining is simulated through the use of the Finite Element Method (FEM). The developed model is able to simulate the presence of the lining rings and the circular joints, considering the vertical buoyant forces applied by the fluid slurry and the reaction to the vertical displacements by the solid slurry together with the surrounding ground. The reference section is the one shown in Fig. 4. In the model, each single lining ring is represented by 4 mono-dimensional elements each 29 cm long; the circular joint is also represented with a mono-dimensional short element, 4 cm long (Fig. 4). All the mono-dimensional elements that represent the structure (lining rings and circular joints) are connected in series through nodes, to which the buoyant forces and the reaction forces by the solid slurry and the surrounding ground are applied. These reaction forces are represented by independent elastic springs (Winkler springs) and linearly depend on the vertical displacement of the lining.

The local stiffness matrix $\left[k_E\right]_i$ of the generic i mono-dimensional element is multiplied by the nodal displacements (vertical displacements v and rotations θ) in order to obtain the nodal forces (the sum of the transversal force V and the bending moment R). The transversal force V at the fluid slurry zone is equal to the vertical load q on the segment multiplied by the average length $l_{av,i}$ of elements adjacent to the node i on both sides, $l_{av,i} = \left(l_{i-1} + l_i\right)/2$, where l_{i-1}, l_i, l_{i+1} are the length of element $i-1$, i, $i+1$. The transversal force V at the solid slurry zone is equal to the Winkler spring stiffness k_w multiplied by the vertical displacement of the node, v_f, which is the last node of the fluid slurry zone, and by the average length of elements adjacent to the node. Due to the vertical displacement

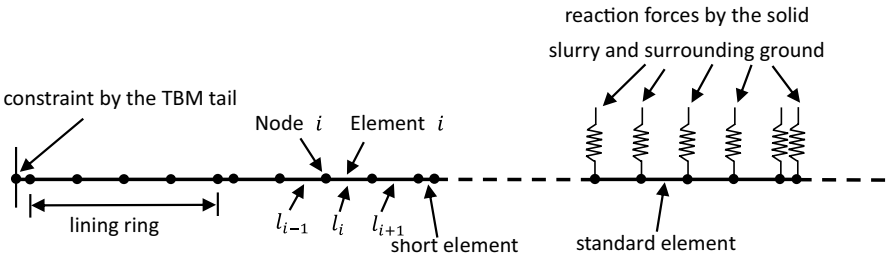


Fig. 4 Adopted scheme of the longitudinal FEM model of the segmental lining in the fluid slurry zone and in the solid slurry one. Standard elements are used to simulate the segment rings and elements of a reduced length (short elements) to simulate circular joints

v_f influencing the nodal forces, an iterative calculation procedure needs to be implemented.

$$\left[k_E\right]_i \cdot \begin{bmatrix} v_{h,i} \\ \theta_{h,i} \\ v_{j,i} \\ \theta_{j,i} \end{bmatrix} = \begin{bmatrix} V_{h,i} \\ R_{h,i} \\ V_{j,i} \\ R_{j,i} \end{bmatrix} \tag{4}$$

where the subscript h refers to the initial node, the subscript j to the final node of the generic i element.

$$\left[k_E\right]_i = \frac{EI}{l^3}\begin{bmatrix} 12 & 6l & -12 & 6l \\ 6l & 4l^2 & -6l & 2l^2 \\ -12 & -6l & 12 & -6l \\ 6l & 2l^2 & -6l & 4l^2 \end{bmatrix} \tag{5}$$

where E and I are the elastic modulus of the material (concrete) and the inertia moment of the element cross-section for a standard element, respectively; l is the length of the standard element. However, for a short element, EI is equal to the equivalent bending stiffness of the joint $(EI)_{eq}$, l is equal to the length of the assumed short element l_{short}.

In order to consider also the influence of the shear deformability of the lining, the local stiffness matrix is modified based on the following equations:

$$\left[k_E\right]_i = \frac{EI}{l^3}\begin{bmatrix} \overbrace{\begin{matrix} \frac{12}{1+\Phi} & \frac{6l}{1+\Phi} \\ \frac{6l}{1+\Phi} & \frac{4+\Phi}{1+\Phi}l^2 \end{matrix}}^{[k]_{i,a}} & \overbrace{\begin{matrix} -\frac{12}{1+\Phi} & \frac{6l}{1+\Phi} \\ -\frac{6l}{1+\Phi} & \frac{2-\Phi}{1+\Phi}l^2 \end{matrix}}^{[k]_{i,b}} \\ \underbrace{\begin{matrix} -\frac{12}{1+\Phi} & -\frac{6l}{1+\Phi} \\ \frac{6l}{1+\Phi} & \frac{2-\Phi}{1+\Phi}l^2 \end{matrix}}_{[k]_{i,c}} & \underbrace{\begin{matrix} \frac{12}{1+\Phi} & -\frac{6l}{1+\Phi} \\ -\frac{6l}{1+\Phi} & \frac{4+\Phi}{1+\Phi}l^2 \end{matrix}}_{[k]_{i,d}} \end{bmatrix} \tag{6}$$

where $[k]_{i,a}$,$[k]_{i,b}$,$[k]_{i,c}$,$[k]_{i,d}$ are the 2×2 sub matrices of $\left[k_E\right]_i$, Φ is the ratio between the bending stiffness and the shear stiffness, and is equal to:

$$\Phi = \frac{12 \cdot EI}{kG \cdot A_T \cdot l^2} \tag{7}$$

where G is shear elastic modulus of concrete, k is the shear coefficient of Timoshenko's beam and is equal to $2\left(1+\nu_{con}\right)/\left(4+3\nu_{con}\right)$ considering the lining as a thin-walled tube (Cowper, 1966), ν_{con} is the Poisson's ratio of concrete, A_T is the lining cross-section area (perpendicular to the tunnel axis). Similarly, the equivalent bending stiffness $(EI)_{eq}$ and the equivalent shear stiffness $\left(kG \cdot A_T\right)_{eq}$ of the circular joint were used to obtain the local stiffness matrix for the short element.

The global stiffness matrix $[K]$ is obtained by composing the local stiffness matrices along the diagonal, adding together the overlapping terms:

$$\begin{bmatrix} k_{1,a} & k_{1,b} & 0 & 0 & \cdots & 0 & 0 \\ k_{1,c} & k_{1,d}+\boldsymbol{k}_{2,a} & \boldsymbol{k}_{2,b} & 0 & \cdots & 0 & 0 \\ 0 & \boldsymbol{k}_{2,c} & \boldsymbol{k}_{2,d}+k_{3,a} & k_{3,b} & \cdots & 0 & 0 \\ 0 & 0 & k_{3,c} & k_{3,d}+\boldsymbol{k}_{4,a} & \cdots & 0 & 0 \\ \vdots & \vdots & \vdots & \vdots & \ddots & 0 & 0 \\ 0 & 0 & 0 & 0 & \cdots & k_{n-1,d}+\boldsymbol{k}_{n,a} & \boldsymbol{k}_{n,b} \\ 0 & 0 & 0 & 0 & \cdots & \boldsymbol{k}_{n,c} & \boldsymbol{k}_{n,d} \end{bmatrix} \cdot \begin{bmatrix} S_1 \\ S_2 \\ S_3 \\ S_4 \\ \vdots \\ S_n \\ S_{n+1} \end{bmatrix} = \begin{bmatrix} F_1 \\ F_2 \\ F_3 \\ F_4 \\ \vdots \\ F_n \\ F_{n+1} \end{bmatrix} \tag{8}$$

where $k_{i,a}$ means $[k]_{i,a}$; S_1, S_2, … S_{n+1} are the sub vectors displacement of each node from the first (on the TBM tail, Node 1) to the final one (Node n + 1); $S_i = \left[v_i \ \theta_i \right]^T$, v_i and θ_i are the vertical displacement and rotation of node i; F_1, F_2, … F_{n+1} are the external forces applied at each node, $F_i = \left[V_i \ R_i \right]^T$, V_i and R_i are the transversal force and the bending moment of node i, respectively.

Considering the effect of normal interaction springs in the nodes of the solid slurry zone, only some values of the global stiffness matrix $[K]$ are modified along the diagonal (alternatively the elements of the diagonal starting from the first to the penultimate). Based on the relationship between the reaction pressure and the transversal displacement of a circular element surrounded by the ground, an adding term of $\left[k_w\right]_{i,a}$ has to be considered and added to the sub matrices $[k]_{i,a}$ of $[K]$:

$$\left[k_w\right]_{i,a} = \begin{bmatrix} k_w \cdot l_{av,i} & 0 \\ 0 & 0 \end{bmatrix} \tag{9}$$

where k_w is the Winkler spring stiffness of the solid slurry and the ground, and is equal to the ratio of q_u/δ_u, where q_u is the ultimate uplift resistance of the solid slurry and the surrounding ground to the lining vertical movement, and δ_u is the ultimate displacement value, equal to 0.02•D for shallow and medium buried tunnels, according to Gong et al. (2018).

$$q_u = D \cdot h_0 \cdot \gamma_G - \frac{\pi}{8} \cdot D^2 \cdot \gamma_G \tag{10}$$

where h_0 is the buried depth of the tunnel axis, γ_G is the bulk density of the ground.

The segment rings are connected by circular joints with bolts; the stiffness of these circular joints is lower than the stiffness of the segment rings. In order to correctly analyses the behaviour of a segment lining, it is necessary to evaluate with a certain precision both the equivalent bending stiffness and the equivalent shear stiffness of the mono-dimensional element that represents the circular joint (short elements in Fig. 4). These equivalent stiffnesses are influenced by the type of joint, such as the number and the diameter of the steel bolts. Moreover, the contact area of two adjacent segments is influenced by the axial force N applied by jacks on the first segment ring at the TBM tail; equivalent stiffnesses of the circular joints increase when the applied axial force increases.

The evaluation of the circular joint equivalent stiffnesses has been developed based on the Timoshenko beam model, considering the yield state of bolts (Cheng et al. 2021; Liao et al. 2008):

With reference to the bending stiffness of the joint, it is possible to evaluate the minimum value of the equivalent elastic modulus E^* of the one-dimensional element that represents it (short element), in the absence of the axial force N applied by the TBM:

$$E^* = E \cdot \frac{l_{short}}{\lambda l_b} \cdot \frac{cos^3\varphi}{cos\varphi + (\pi/2 + \varphi) \cdot sin\varphi} \tag{11}$$

where l_b is the bolt length, λ is a coefficient that is multiplied by l_b in order to obtain the influencing length of the joint, λl_b, and is about 0.5 based on the research of a shield tunnel in Shanghai metro, China (Xu 2005). The influencing length λl_b is difficult to obtain based on a precise equation; l_b is assumed as the projection length of the curved bolt (0.4 m with an arc length 0.53 m for the cited case) so as to get the minimum value of the equivalent elastic modulus. For the purpose of knowing the influence of the equivalent bending stiffness on the behaviour of the segmental lining, a sensitivity analysis was carried out in the paragraph 5. Here, φ is the angle describing the location of the neutral axis (Cheng et al. 2021; Liao et al. 2008):

$$\varphi + cot\varphi = \pi \cdot \left(\frac{1}{2} + \frac{n_b \cdot E_{st} \cdot A_b}{E \cdot A_T} \right) \tag{12}$$

where n_b is the number of bolts connecting the circular joint, E_{st} is the elastic modulus of the steel bolt, A_b is the cross-section area of the bolt, $A_b = (\pi/4) \cdot \Phi_b^2$, Φ_b is the bolt diameter, A_T is the cross-section area of the segmental lining, $A_T = (\pi/4) \cdot \left[D^2 - (D - 2t)^2\right]$, t is the lining thickness.

Li et al. (2019) researched the influence of the longitudinal axial forces N on the bending behaviour of a circular joint, using the following ratio parameter ω:

$$\omega = \frac{N \cdot r}{2 \cdot M} \tag{13}$$

where N is the axial force applied by the TBM jacks to the segmental lining, M is the bending moment

induced in the circular joint by the applied buoyant forces, r is the distance between the longitudinal bolts and the tunnel axis.

The effective value of the equivalent elastic modulus of the short element can be determined by the following expression as the ω varies, and therefore as the force N applied by the TBM varies:

$$E_{eq} = E^* + (E - E^*) \cdot \alpha \tag{14}$$

where α is a dimensionless coefficient from 0 to 1, and its value depend on the parameter ω:

$$\begin{cases} \alpha = \omega \ \ \omega \le 1 (\text{case of an open joint}) \\ \alpha = 1 \ \ \omega > 1 (\text{case of a closed joint}) \end{cases} \tag{15}$$

As regards the shear stiffness of the short element representing the circular joint, it is possible to write the following expression (Cheng et al. 2021) for the product $\left(kG \cdot A_T\right)$ equivalent:

$$\left(kG \cdot A_T\right)_{eq} = \frac{Q}{u_{max}} \cdot l_{short} \tag{16}$$

where Q is the ultimate shear force of the circular joint when the bolts reach their limit shear stress:

$$Q = \frac{\sqrt{3}}{16} \cdot n_b \cdot \pi \cdot \Phi_b^2 \cdot \sigma_y \tag{17}$$

σ_y is the steel yield stress of the bolt. u_{max} is the maximum relative displacement of the circular joint, when the ultimate shear force Q is reached in the circular joint. This displacement is the sum of the gap distance between the bar and the hole where it is inserted and the deformation of the bolt when a shear force is applied on it:

$$u_{max} = \left(\phi_h - \phi_b\right) + l_b \cdot tan\left(\frac{Q}{n_b \cdot k_b \cdot G_{st} \cdot A_b}\right) \tag{18}$$

where ϕ_h is the diameter of the bolt hole, k_b is Timoshenko shear coefficient of the bolt (for a circular section: $k_b = 6\left(1 + \nu_{st}\right)/\left(7 + 6\nu_{st}\right)$ (Cowper, 1966)), G_{st} is the steel shear elastic modulus, $G_{st} = E_{st}/\left(2\left(1 + \nu_{st}\right)\right)$, ν_{st} is the Poisson's ratio of steel.

Proceeding with the substitutions, the equivalent shear stiffness of a circular joint can be obtained:

$$\left(kG \cdot A_T\right)_{eq} = \frac{\sqrt{3} \cdot n_b \cdot \pi \cdot \Phi_b^2 \cdot \sigma_y}{16 \cdot \left[\left(\phi_h - \phi_b\right) + l_b \cdot tan\left(\frac{\sqrt{3} \cdot \sigma_y}{4 \cdot k_b \cdot G_{st}}\right)\right]} \cdot l_{short} \tag{19}$$

4 Analysis of the Risk of Damage of the Lining on the Basis of the Induced Global State of Stress

Based on the developed numerical model, the bending moment M and shear force T in the segmental lining along the tunnel axis can be obtained. And then, the stress state in the concrete and in the connecting bolts of circular joints is calculated combining the normal force N applied by the TBM jacks and the radial pressure of slurry p on the outer border of the lining in the fluid zone (Fig. 5).

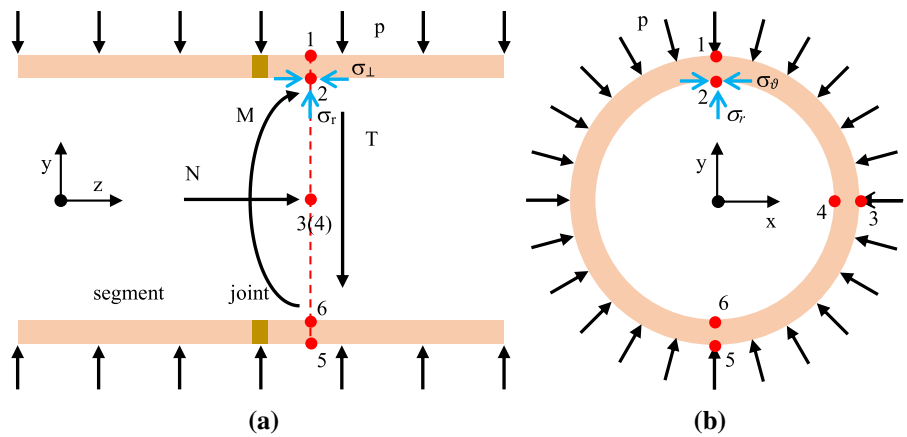


Fig. 5 The applied loads and the stress state in the segmental lining. Key: **a** longitudinal view, **b** transversal view. Six different critical points are shown where the stress state has been evaluated

In order to evaluated the maximum principal stresses in the segment lining, six special points were chosen to develop the calculation (Fig. 5). The main procedure can be concluded in four steps. Firstly, the special transversal sections can be chosen based on the distribution of moments and shear forces along the tunnel axis (Para. 3). Secondly, the special points are defined in the transversal sections (point from 1 to 6). Thirdly, combining the force N and T, the moment M and the pressure p, the stress state is there calculated. Finally, the damage risk level of the segment lining can be obtained by comparing the principal stresses with the concrete strength or the steel yield stress.

4.1 The Stress State Inside the Segment of a Lining

Based on the mechanics principles and using a cylindrical coordinate system, the stress state of a point can be described by the longitudinal normal stress $\sigma_{\perp}$, the radial normal stress σ_r, the circumferential normal stress σ_{ϑ}.

The longitudinal normal stress of the segment is obtained from the axial force and the bending moment of the transversal section.

$$\sigma_{\perp} = \frac{N}{A_T} \pm \frac{M}{I} \cdot r \tag{20}$$

Based on the Lamé's equations and considering the existing boundary conditions, the radial normal stress σ_r and the circumferential normal stress σ_{ϑ} can be obtained using the following equations:

$$\begin{cases} \sigma_r = p & r = R \\ \sigma_r = 0 & r = R - t \end{cases} \tag{21}$$

$$\begin{cases} \sigma_{\vartheta} = p \cdot \frac{R^2 + (R-t)^2}{R^2 - (R-t)^2} & r = R \\ \sigma_{\vartheta} = p \cdot \frac{2 \cdot R^2}{R^2 - (R-t)^2} & r = R - t \end{cases} . \tag{22}$$

4.2 The Stress State of Segments Joint

When a circular joint rotate due to a moment, the contact face can be divided into two zones: the compression zone and the detached one (Fig. 6b). Due to the opening of the joint, the normal stress in the detached zone is zero, and the compressive stress in the bolts of the compression zone are also equal to zero. Therefore, the absence of a normal tensile stress in the joint will lead to an increase of the compressive stresses in the concrete with respect to the state of stress of the transversal section of the segment.

The deformation of a circular joint can be described by the rotation angle θ and the location of the neutral axis y_n (Fig. 6a). Based on the assumption that the joint contact face remains a plane after the deformation, the stress state on the concrete can be obtained, together with the tensile stress state of all the bolts in the detached zone.

The tensile stress of the generic bolt i ($\sigma_{b,i}$) can be obtained by the strain and the steel elastic modulus when the bolt stress is less than the yield stress σ_y.

$$\sigma_{b,i} = \frac{2 \cdot (y_i - y_n) \cdot tan(\theta)}{l_b} \cdot E_{st} \tag{23}$$

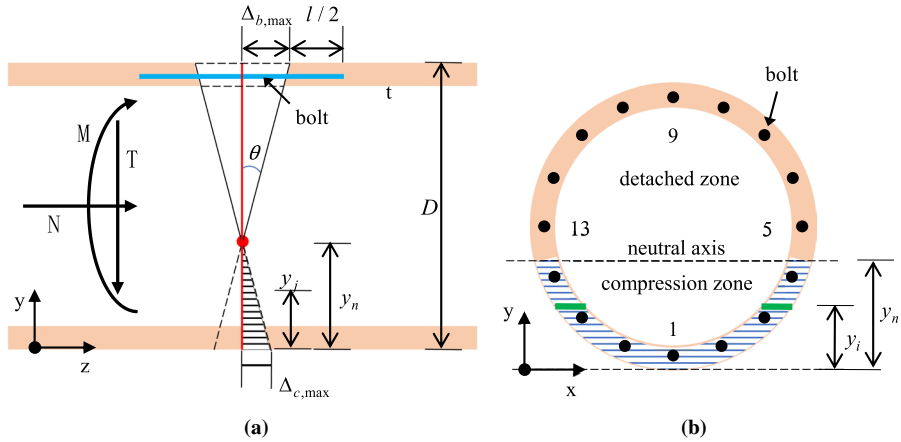


Fig. 6 The tensional and deformative condition of a circular joint when a bending moment M and a normal force N are present (case of 16 bolts connecting the circular joint). **a** longitudinal view, **b** transversal view

where y_i is the location of bolt i with respect to the origin, y_n is the location of the neutral axis.

The trend of the normal stress at the contact face in the compression zone can be assumed linear by the following expression:

$$\sigma_{c,j} = \sigma_{c,\max} \cdot \frac{\left(y_n - y_j\right)}{y_n} \tag{24}$$

where y_j is location of the calculation point. The maximum compression stress $\sigma_{c,max}$ can be determined by considering the displacement of the extreme point of the compression zone and the stiffness of the concrete face of the joint k_c:

$$\sigma_{c,max} = k_c \cdot y_n \cdot \tan(\theta) \tag{25}$$

where: k_c is the compression stiffness of the joint face based on the Winkler theory (Canadian Geotechnical Society 2006), which can be estimated by the following expression:

$$k_c = \frac{4 \cdot G}{\pi \cdot R_{eq} \cdot \left(1 - \nu_{con}\right)} \tag{26}$$

where R_{eq} is the equivalent radius obtained by the ratio $\sqrt{A_c/\pi}$, A_c is the area of compression zone of the circular joint.

The angle θ and the value of y_n are determined on the basis of the bending moment M and normal force N acting on the considered circular joint: they are varied in an iterative procedure till to reach the condition for which the compressive stresses in the contact zone of the joint and the tensile forces in the bolts produce the same moment M and the same normal force N acting on the joint.

The compressive stresses in the contact zone are the longitudinal stresses $\sigma_\perp$ of the circular joint. When the area of the detached zone is equal to nil, the longitudinal stresses of the circular joint are calculated using the equation for the segment. The radial stresses and circumferential ones can be calculated in the same way previously described for the segment. Because the stress state of point 1 and 5 is at its maximum level of the cross section (Fig. 5), and there is no shear stress at these two points, the equation of a shear stress is not present. Table 3 list the equations of the stress state of the critical point.

4.3 The Determination of the Safety Factors

Based on the stress state evaluation in the concrete for segments and circular joints, the three principal stresses (σ_1, σ_2, and σ_3) are determined; a greater interest exists in the evaluation of σ_1 and σ_3:

$$\sigma_1 = \max\left(\sigma_r, \sigma_\vartheta, \sigma_\perp\right) \tag{27}$$

$$\sigma_3 = \min\left(\sigma_r, \sigma_\vartheta, \sigma_\perp\right) \tag{28}$$

In fact, considering the concrete strength subjected to the Mohr–Coulomb failure criterion, the limit

Table 3 the equations of the stress state for the six critical point in the segmental lining

Point No	σ_r	σ_ϑ	$\sigma_\perp$(Closing joint and Segment)	$\sigma_\perp$(Opening joint)
1	p	$p \cdot \frac{R^2+(R-t)^2}{R^2-(R-t)^2}$	$\frac{N}{A_T} - \frac{M}{I} \cdot R$	0
2	0	$p \cdot \frac{2 \cdot R^2}{R^2-(R-t)^2}$	$\frac{N}{A_T} - \frac{M}{I} \cdot (R-t)$	$\sigma_{c,max} \cdot \frac{(y_n-2R+t)}{y_n}$ $y_n > 2R-t$
3	p	$p \cdot \frac{R^2+(R-t)^2}{R^2-(R-t)^2}$	$\frac{N}{A_T}$	$\sigma_{c,max} \cdot \frac{(y_n-R)}{y_n}$ $y_n > R$
4	0	$p \cdot \frac{2 \cdot R^2}{R^2-(R-t)^2}$	$\frac{N}{A_T}$	$\sigma_{c,max} \cdot \frac{(y_n-R)}{y_n}$ $y_n > R$
5	p	$p \cdot \frac{R^2+(R-t)^2}{R^2-(R-t)^2}$	$\frac{N}{A_T} + \frac{M}{I} \cdot R$	$\sigma_{c,max}$
6	0	$p \cdot \frac{2 \cdot R^2}{R^2-(R-t)^2}$	$\frac{N}{A_T} + \frac{M}{I} \cdot (R-t)$	$\sigma_{c,max} \cdot \frac{(y_n-t)}{y_n}$ $y_n > t$

Where the compression zone is assumed below the neutral axis and the detached zone is above it. If the joint opens with the application of the bending moment M and normal force N, the longitudinal normal stress $\sigma_\perp$ is calculated using the equation of the table when y_n satisfied the corresponding conditions, otherwise $\sigma_\perp$ is equal to 0. When the joint is closed, the longitudinal normal stress $\sigma_\perp$ is calculated using the equation of the penultimate column.

major principal stress for the concrete can be obtained from the following equation:

$$\sigma_{1,lim} = 2 \cdot c_{con} \cdot \frac{cos\varphi_{con}}{1 - sin\varphi_{con}} + \sigma_3 \cdot \frac{1 + sin\varphi_{con}}{1 - sin\varphi_{con}} \quad (29)$$

where c_{con} is the cohesion of concrete and φ_{con} is the internal friction angle of concrete; the typical values of the cohesion of concrete (C50 type) is about 25.75 MPa and of the internal friction angle is about 34.25° (Tu et al. 2020).

The safety factor of concrete can be defined by the ratio of the limit major principal stress divided by the existing major principle stress.

$$F_{s,con} = \frac{\sigma_{1,lim}}{\sigma_1} \quad (30)$$

When the circular joint rotates and opens, the bolt which has a largest distance from the neutral axis in the detached zone undergoes the maximum tensile deformation, and is the critical bolt for the safety evaluations of segmental lining, such as the bolt 9 in Fig. 6. As regards the critical bolts of the circular joint stressed in traction, it is possible to evaluate a safety factor with regard to the elastic limit, through the following equation, knowing the values of θ and y_n for the specific circular joint:

$$F_{s,bolt} = \frac{\sigma_y}{\max\left(\sigma_{b,i)}\right)} = \frac{\sigma_y \cdot l_b}{2 \cdot \left[(D - t/2) - y_n\right] \cdot tan(\theta) \cdot E_{st}}. \quad (31)$$

5 Application of the Proposed Model to a Real Case

The proposed FEM model of the longitudinal analysis of the segmental lining was applied to a metro shield tunnel which was excavated by an EPBS (a type of Tunnel Boring Machine) with a shield tail diameter of 6.34 m in Ningbo (China). The concrete segmental lining with a 1.2 m rings width has an outer diameter of 6.2 m and a thickness of 0.35 m. The lining was made of a C50 concrete (Young's Modulus 3.45×10^4 MPa, Poisson's ratio 0.167 and unit weight 25 kN/m^3). In order to connect the segmental lining with bolts, bolt holes with a 39 mm diameter was reserved during pouring. The shield tunnel was built in a soft soil, and the uplift of the segmental lining was detectable during the tunnel excavation. Zhou and Ji (2014) measured this upward movement and found that the maximum value achieved 120 mm at some segments. The adopted basic parameters of bolts are listed in the Table 4, on the basis of the available documents in the scientific literature (Chen et al. 2018; Ji et al. 2014, 2013; Ye et al. 2014; Zhou et al. 2013; Zhou and Ji, 2014).

Based on preliminary field test results, the influence of the vertical component of jack thrust, of the pressure chamber and of the advance rate of the TBM on the lining uplift was insignificant and for this reason these aspects were neglected in the subsequent analysis; the slurry characteristics, on the contrary, have a significant influence (Zhou and Ji 2014). The composition of the adopted slurry include cement, bentonite, sand, fly ash, quick lime, water and admixture. The quality proportion (kg) of the adopted slurry is: 100: 300: 2750: 700: 100: 900: 1 (for GC1 type); 150: 300: 2750: 650: 100: 900: 1 (for GC2 type), and 250: 300: 2750: 650: 0: 900: 1(for GC3 type). The slurry properties, the grouting parameters and the measured uplift displacements of the segmental lining are listed in the Table 5. The density of the slurry is about 1938 kg/m^3 for all the considered types.

The tunnel depth is about 15–16 m from the surface (Ji et al. 2013) and 8–10 lining rings were realised per day: it means that an average excavation

Table 4 Parameters of the longitudinal steel bolts connecting segmental rings at the studied Ningbo tunnel

External Bar Diameter (mm)	Nominal Stress Area (mm^2)	Equivalent Bar Diameter (mm)	Longitudinal Projection Length (mm)	Total Arc length (mm)
30	561	26.73	400	530
Total number	Steel Young's Modulus (MPa)	Steel Poisson's ratio (−)	Steel yield stress (MPa)	Steel ultimate stress (MPa)
16	2.06×10^5	0.3	640	800

Table 5 Main properties of the adopted slurries and the grouting parameters

Type of slurry	hardening time (h)	compressive strength (1d) (MPa)	grouting volume (m^3)	uplift stabilizing time (h)	average uplift displacement (mm)
GC1	16	0.06	2.58	35	50.6
GC2	15	0.08	2.72	25	43.6
GC3	12.5	0.11	2.75	20	32.1

speed of 0.4–0.5 m/h was reached (Chen et al. 2018). An average value of 0.46 m/h was considered in the calculation with the proposed FEM numerical model.

For the three adopted types of slurry, the trend of vertical displacements of the segmental lining was calculated and then it was compared with the measured average values. A good concordance was obtained between the calculated values and the measured ones (Fig. 7).

From the Fig. 7 it is possible to note how, when the TBM keeps the same average speed, the hardening time of the slurry is a key parameter influencing the trend of vertical displacements of the segmental lining. The larger increase in the vertical displacements is at the circular joints (the increase of the vertical displacements inside each segment is very small if compared with the joint dislocation), and the dislocation between two adjacent segmental rings decreases with the increase of the distance from the shield tail. Different from the equivalent continuous beam model approach based on the Timoshenko beam and the Euler–Bernoulli beam theory, the proposed simplified FEM model can correctly evaluate the discontinuous and complex deformation trend of a segmental lining when buoyancy forces are present close to the TBM tail.

Then, a sensitivity analysis was carried out changing the TBM average speed, that is a key parameter influencing the length of the fluid slurry zone, together with the hardening time of the slurry. Figure 8 shows the maximum vertical displacement for the average TBM speed in the range 0.4–0.5 m/h for a hardening time of the slurry of 15 h (considered type of slurry GC2). As to be expected, the average excavation speed has a significant role on the uplift displacements of the segmental lining. Due to the length of each segment (1.2 m) and the presence of circular joints along the tunnel axis, the maximum vertical displacement trend is not a straight line. Based on the measured vertical displacement for GC2 slurry type, an excavation TBM speed of 0.4655 m/h can be obtained by the anti-analysis method with the fitted curve. It is possible to see how there is a 34.3% decrease of the maximum vertical displacement when

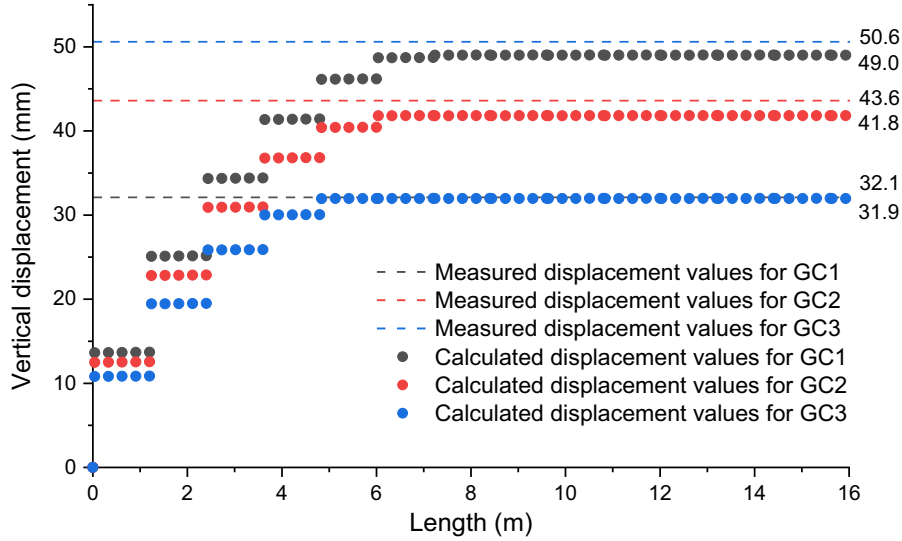


Fig. 7 Comparison of the calculated vertical displacements using the proposed numerical model with the measured values (Zhou and Ji 2014), for the three adopted types of slurry (GC1, GC2 and GC3) at the studied case (Ningbo tunnel)

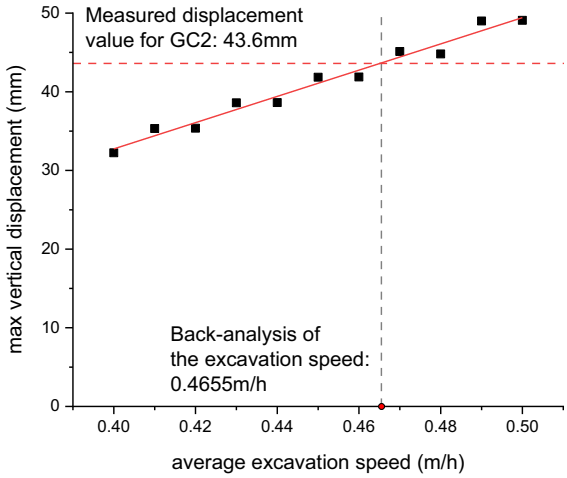


Fig. 8 Results of the sensitivity analysis of the average TBM speed in terms of the maximum vertical displacement of the segmental lining along the tunnel axis (for GC2 slurry type), using the proposed numerical model

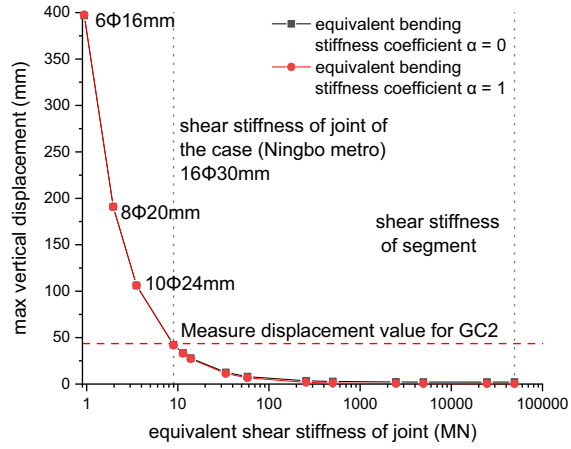


Fig. 9 Sensitivity analysis on the equivalent stiffnesses values of the circular joint for the examined case of the Ningbo tunnel in China. Key: the equivalent bending stiffness coefficient α refers to the two extreme cases of a joint with $N=0$ ($\alpha=0$) and of a segment ring ($\alpha=1$); the equivalent shear stiffness refers to the studied case (16 bolts with a diameter of 30 mm) and to other assumed cases. The dashed red line refers to the measured displacement at the studied case for a GC2 type of slurry, with a maximum vertical displacement of the segmental lining close to 45 mm

the average TBM speed is reduced by 20% (from 0.5 to 0.4 m/h). However, shortening the hardening time is another way to control the vertical displacements of the segmental lining and also the bending moments developed along the longitudinal direction.

The segments discontinuity is characterized by the equivalent stiffness values of the circular joints (equivalent bending stiffness and equivalent shear stiffness). However, the continuous Timoshenko beam approach simply considers an equivalent stiffness for the whole lining based on correcting factors of the stiffness of the concrete segment rings (Cheng et al. 2021; Wu et al. 2015). In the proposed model, it is possible to define equivalent stiffness values for each circular joint of the lining, on the basis of the induced moments and rotations: where small deformations and rotations are calculated, for example in the solid slurry zone, the equivalent stiffness of the joint can be the same of the concrete segment one. Changing the equivalent bending stiffness coefficient from 0 (0%) to 1 (100%), the bending equivalent stiffness will enhance from the weak joint stiffness (without any axial force N applied to it), to the concrete segment stiffness. On the other hand, three different combinations of bolts (6Φ16mm, 8Φ20mm, 10Φ24mm) were also considered. The maximum vertical displacement of the segment lining with different equivalent shear stiffnesses of the circular joint was also calculated and the results of the sensitivity analysis is shown in Fig. 9.

From Fig. 9, it is possible to see how the equivalent shear stiffness of the circular joint is a main parameter influencing the vertical displacements of the lining. With an increase of the equivalent shear stiffness, the maximum vertical displacement decreases sharply, till to reach an asymptotic value on the horizontal axis. When the equivalent shear stiffness is more than 400MN, the maximum vertical displacement roughly keeps it steady and reaches a nil value. The equivalent bending stiffness of the joint results to have a small impact on the maximum vertical displacement of the lining. When the equivalent shear stiffness of the circular joint is small, the maximum vertical displacement is more or less the same considering the two different considered equivalent bending stiffness. On the basis of this analysis it is possible to assert that the shear stiffness of the circular joint represents a fundamental characteristic of the lining able to greatly influence the behaviour of the segmental lining when buoyancy forces are present in the fluid slurry zone. So, in order to control the vertical displacements of the segment lining, enhancing the shear stiffness of

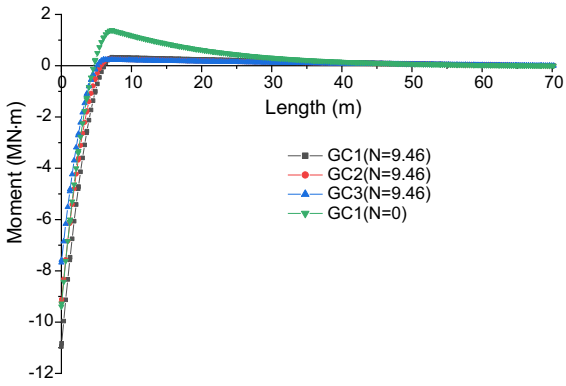


Fig. 10 Trend of the bending moments along the segmental lining (longitudinal direction) of the studied case (Ningbo metro tunnel), for different values of the jack thrust and types of slurry. Key: the length is measured by the TBM tail (initial point of the segmental lining)

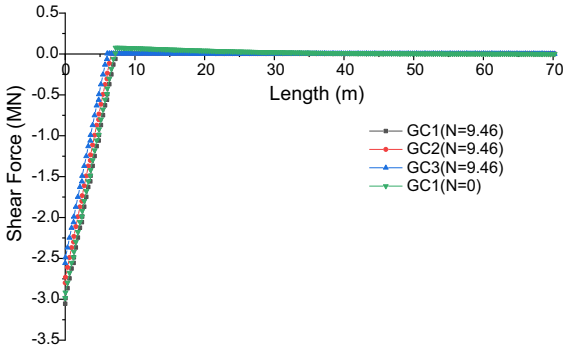


Fig. 11 Trend of the shear forces along the segmental lining (longitudinal direction) of the studied case (Ningbo metro tunnel), for different values of the jack thrust and types of slurry. Key: the length is measured by the TBM tail (initial point of the segmental lining)

the circular joints is an efficient aspect of optimizing the segmental lining.

The normal force is applied by the jack thrust and can change during the excavation and segment assembling steps. Because the maximum thrust reached in the studied case was 9.46 MN (Zhou and Ji 2014), the normal force N applied to the lining was considered changing from 0 to 9.46 MN. When the normal force N respectively is equal to 0 and 9.46MN, the bending moments and the shear forces in the segmental lining along the tunnel axis are shown in Figs. 10 and 11. From the analysis of these two figures, the first circular joint close to the TBM tail has the maximum shear force and also the maximum bending moment. The maximum shear force is 2.98MN and 3.05 MN for the normal force $N=0$ and $N=9.46$MN, respectively, and the maximum moment is 9.39MN•m and 10.95 MN•m (in the case of the adopted slurry type GC1). The grouting pressure p around the segmental lining was 0.32 MPa in the fluid zone. When the normal force is nil ($N=0$), the maximum tensile stress in the critical bolt is 504.23 MPa. The calculation results of the stress state in the segmental lining for the six critical point is listed in Table 6.

Table 6 shows that maximum compressive normal stress is 3.2 MPa at the critical point 5 in a circular joint when the axial normal force N is equal 0, and the minimum normal stress is -1.05 MPa (tensile stress) at the critical point 1 inside the segmental lining when the axial normal force N is equal to 0. So, these two points are the key point in the studied case for the safety analysis. Based on the Mohr–Coulomb failure criterion, the limit stress $\sigma_{1,\mathrm{lim}}$ for a C50 concrete can be evaluated in 98.51 MPa ($\sigma_1=3.2$ MPa, $\sigma_3=0.32$ MPa). The safety factor with respect to the

Table 6 Calculation results of the stress state for the six critical point in the segmental lining

Critical Point No	σ_r(MPa)	σ_ϑ(MPa)	$\sigma_\perp$(MPa) ($N=9.46$MN, M = 10.95 MN•m) (Closing joint and Segment)	$\sigma_\perp$(MPa)($N=0$, M = 9.39 MN•m)	
				Segment	Opening joint
1	0.32	2.68	0.24	**−1.05**	0
2	0	3.00	0.38	−0.94	0
3	0.32	2.68	1.47	0	0
4	0	3.00	1.47	0	0
5	0.32	2.68	2.70	1.05	**3.20**
6	0	3.00	2.56	0.93	1.65

damage of concrete on the first circular joint is evaluated by the ratio 98.51/3.2 MPa, that is 30.78. Similarly, the limit stress $\sigma_{1,\lim}$ is equal to 93.62 MPa for the point 1 (σ_1=2.68 MPa, σ_3=-1.05 MPa), and the ratio of safety factor is equal to 34.93.

Due to the fact that also the maximum tensile stress calculated in the bolts (504.32 MPa) is smaller than the steel yield stress (σ_y=640Mpa, $F_{s,bolt}$=1.26), the concrete and the bolts result to be both in a safe condition for the studied case.

6 Conclusions

Segmental lining is a type of support widely used in tunnels to ensure stability when a TBM excavation machine is used. This support structure is made up of segmental rings and circular joints that alternate in the longitudinal direction starting from the TBM tail. A specific material (slurry) is generally injected between the external profile of the segmental lining and the tunnel wall, and important buoyancy forces are applied to the segmental lining where the slurry is fluid, which cause the lining deformation along the longitudinal direction, induce the appearance of bending moments and shear forces along the longitudinal direction from the TBM tail, and can lead to a damage of the segmental lining.

Due to the type of structure, the analysis of displacements and stresses in the segmental lining is very complex. In order to effectively study the problem, a specific numerical model has been developed with the Finite Element Method (FEM). This numerical model makes it possible to take into account all the fundamental aspects of the phenomenon and in particular the evolution of the characteristics of the filling material (slurry) in the gap between the external profile of the segmental lining and the tunnel wall, the extent of the forces buoyancy of the segmental lining, the nature and characteristics of the segmental rings and circular joints, the speed of the TBM and the forces applied by the TBM tail to the first lining ring.

Thanks to the developed numerical model, it is possible to carry out an accurate assessment of the stress state in the segmental lining and in the steel bolts that guarantee the connection between different segmental rings. This evaluation allows a correct design of the support system taking into account all the aspects that affect the evolution of the displacements and bending moments along the tunnel axis.

The application of the proposed numerical model to a real case (the Ningbo metro tunnel) made it possible to compare the results of the calculation with the in situ measurements, obtaining satisfactory results. Some sensitivity analyzes developed on the studied case made allowed to detect the importance of some parameters on the behavior of the segmental lining, such as the advancement speed of the TBM, the shear stiffness of the circular joints and the axial forces applied by the TBM tail to the first segmental ring.

However, in order to take the advantage of this model considering the influence of the individual joints and more accurately analyze the segmental lining deformation along the longitudinal direction, a more detailed evaluation for the joint stiffness in the process of its deformation is necessary in future studies.

Acknowledgements This study was financially supported by the National Natural Science Foundation of China (No. 51878060) and the Fundamental Research Funds for the Central Universities, CHD (No. 300102212702), and this support is gratefully acknowledged. The first author also would like to appreciate the scholarship from China Scholarship Council (Grant No. 202106560030) for his study in Politecnico di Torino.

Authors Contribution XH and PO: Conceptualization, Data curation, Investigation, Methodology, Writing; FY: Supervision, Validation.

Funding Open access funding provided by Politecnico di Torino within the CRUI-CARE Agreement.

Data Availability Enquiries about data availability should be directed to the authors.

Declarations

Conflict of interest The authors declare that they have no known competing financial interests or personal relationships that could have appeared to influence the work reported in this paper.

Open Access This article is licensed under a Creative Commons Attribution 4.0 International License, which permits use, sharing, adaptation, distribution and reproduction in any medium or format, as long as you give appropriate credit to the original author(s) and the source, provide a link to the Creative Commons licence, and indicate if changes were made. The images or other third party material in this article are included in the article's Creative Commons licence, unless indicated otherwise in a credit line to the material. If material is not included in the article's Creative Commons licence and your

intended use is not permitted by statutory regulation or exceeds the permitted use, you will need to obtain permission directly from the copyright holder. To view a copy of this licence, visit http://creativecommons.org/licenses/by/4.0/.

References

Arnau O, Molins C (2012) Three dimensional structural response of segmental tunnel linings. Eng Struct 44:210–221

Bezuijen A, Talmon AM, Kaalberg FJ, Plugge R (2004) Field measurements of grout pressures during tunnelling of the sophia rail tunnel. Soils Found 44:39–48

Canadian Geotechnical Society (2006) Canadian Foundation Engineering Manual, 4th Edition ed.

Chaipanna P, Jongpradist P (2019) 3D response analysis of a shield tunnel segmental lining during construction and a parametric study using the ground-spring model. Tunn Undergr Space Technol 90:369–382

Chen RP, Meng FY, Ye YH, Liu Y (2018) Numerical simulation of the uplift behavior of shield tunnel during construction stage. Soils Found 58:370–381

Cheng HZ, Chen RP, Wu HN, Meng FY, Yi YL (2021) General solutions for the longitudinal deformation of shield tunnels with multiple discontinuities in strata. Tunn Undergr Space Technol 107:103652

Cheng HZ, Chen RP, Wu HP, Meng FY (2020) A simplified method for estimating the longitudinal and circumferential behaviors of the shield-driven tunnel adjacent to a braced excavation. Comput Geotech 123:103595

China (2009) Standard for test method of basic properties of construction mortar (JGJ/T 70-2009). China Architecture and Building Press **(in Chinese)**

Cowper GR (1966) The shear coefficient in Timoshenko's beam theory. J Appl Mech 6:335–340

Dastjerdy B, Hasanpour R, Chakeri H (2018) Cracking problems in the segments of Tabriz Metro tunnel: a 3D computational study. Geotech Geol Eng 36:1959–1974

Do N-A, Dias D, Oreste P, Djeran-Maigre I (2013) 3D modelling for mechanized tunnelling in soft ground-influence of the constitutive model. Am J Appl Sci 10(8):863–875

Do N-A, Dias D, Oreste P, Djeran-Maigre I (2014) The behaviour of the segmental tunnel lining studied by the hyperstatic reaction method. Eur J Environ Civ Eng 18(4):489–510

Do N-A, Dias D, Oreste P, Djeran-Maigre I (2015) Behaviour of segmental tunnel linings under seismic loads studied with the hyperstatic reaction method. Soil Dyn Earthq Eng 79:108–117

Dong XL, Geng DX, Jiang YL, Liao YQ (2021) Effect of admixtures on mechanical properties of synchronous grouting materials in water-rich composite stratum. Constr Technol 50:18–22

Gong Q, Zhao Y, Zhou J, Zhou S (2018) Uplift resistance and progressive failure mechanisms of metro shield tunnel in soft clay. Tunn Undergr Space Technol 82:222–234

Han L, Ye G-L, Chen J-J, Xia X-H, Wang J-H (2017) Pressures on the lining of a large shield tunnel with a small overburden: a case study. Tunn Undergr Space Technol 64:1–9

He S, Lai J, Wang L, Wang K (2020) A literature review on properties and applications of grouts for shield tunnel. Constr Build Mater 239:117782

Huang X, Huang HW, Zhang J (2012) Flattening of jointed shield-driven tunnel induced by longitudinal differential settlements. Tunn Undergr Space Technol 31:20–32

Innaurato N, Oggeri C, Oreste P, Vinai R (2011) Laboratory tests to study the influence of rock stress confinement on the performances of TBM discs in tunnels. Int J Miner Metall Mater 18:253–259

Ji C, Wang PX, Li X, Di HG (2014) Weight analysis of segment up-foloating factors during metro shield tunnel construction in soft stratum. Mod Tunn Technol 51:164–171 **(in Chinese)**

Ji C, Zhou SH, Xu K, Li XL (2013) Field test research on influence factor of upward moving of shield tunnel segments during construction. Chin J Rock Mech Eng 32:3619–3626 **(in Chinese)**

Koizumi A, Murakami H, Nishino K (1988) Study on the analytical model of shield tunnel in longitudianl direction. J Jpn Soc Civ Eng 394:79–88

Li XJ, Zhou XZ, Hong BC, Zhu HH (2019) Experimental and analytical study on longitudinal bending behavior of shield tunnel subjected to longitudinal axial forces. Tunn Undergr Space Technol 86:128–137

Liang JH (2006) Study on the proportion of backfill-grouting materials and grout deformation properties of shield tunnel. Hohai University, Nanjing **(in Chinese)**

Liang X (2009) Study of material performance and material ratio design in synchronized grouting technology for shield tunneling on watery Strata. Chang'an University, Xi'an, China **(in Chinese)**

Liang X, Ying K, Ye F, Su E, Xia T, Han X (2022) Selection of backfill grouting materials and ratios for shield tunnel considering stratum suitability. Constr Build Mater 314:125431

Liao SM, Peng FL, Shen SL (2008) Analysis of shearing effect on tunnel induced by load transfer along longitudinal direction. Tunn Undergr Space Technol 23:421–430

Liu DJ, Tian C, Wang F, Hu QF, Zuo JP (2021a) Longitudinal structural deformation mechanism of shield tunnel linings considering shearing dislocation of circumferential joints. Comput Geotech 139:15

Liu J, Shi C, Lei M, Wang Z, Cao C, Lin Y (2021b) A study on damage mechanism modelling of shield tunnel under unloading based on damage–plasticity model of concrete. Eng Fail Anal 123:105261

Liu J, Shi C, Wang Z, Lei M, Zhao D, Cao C (2021c) Damage mechanism modelling of shield tunnel with longitudinal differential deformation based on elastoplastic damage model. Tunn Undergr Space Technol 113:103952

Mahmoodzadeh F, Chidiac SE (2013) Rheological models for predicting plastic viscosity and yield stress of fresh concrete. Cem Concr Res 49:1–9

Mao J, Yuan D, Jin D, Zeng J (2020) Optimization and application of backfill grouting material for submarine tunnel. Constr Build Mater 265:120281

Oreste P (2013) Face stabilization of deep tunnels using longitudinal fibreglass dowels. Int J Rock Mech Min Sci 58:127–140

Peila D, Borio L, Pelizza S (2011) The behaviour of a two-componenet back-filling grout used in a tunnel-boring machine. Acta Geotech Slov 8:11

Peila D, Oreste PP, Rabajoli G, Trabucco E (1995) The pretunnel method, a new Italian technology for full-face tunnel excavation: a numerical approach to design. Tunn Undergr Space Technol 10(3):367–374

Pelizza S, Oreste P, Peila D, Oggeri C (2000) Stability analysis of a large cavern in italy for quarrying exploitation of a pink marble. Tunn Undergr Space Technol 15:421–435

Shiba Y, Kawashima K, Obinata N, Kano T (1988) An evaluation method of longitudinal stiffness of shield tunnel linings for application to seismic response analyses. J Jpn Soc Civ Eng 1988(398):319–327

Spagnoli G, Oreste P, Bianco LL (2016) New equations for estimating radial loads on deep shaft linings in weak rocks. Int J Geomech 16(6):06016006

Talmon AM, Bezuijen A (2013) Analytical model for the beam action of a tunnel lining during construction. Int J Numer Anal Methods Geomech 37:181–200

Tian K (2007) Study and application on high property grouting material used in synchronous grouting of shield tunnelling. Wuhan University of Technology, Wuhan, China **(in Chinese)**

Todaro C, Godio A, Martinelli D, Peila D (2020) Ultrasonic measurements for assessing the elastic parameters of two-component grout used in full-face mechanized tunnelling. Tunn Undergr Space Technol 106:103630

Tu H, Zhou H, Lu J, Gao Y, Shi L (2020) Elastoplastic coupling analysis of high-strength concrete based on tests and the Mohr-Coulomb criterion. Constr Build Mater 255:119375

Wang S, He C, Nie L, Zhang G (2019) Study on the long-term performance of cement-sodium silicate grout and its impact on segment lining structure in synchronous backfill grouting of shield tunnels. Tunn Undergr Space Technol 92:103015

Wang S, Liu C, Shao Z, Ma G, He C (2020) Experimental study on damage evolution characteristics of segment structure of shield tunnel with cracks based on acoustic emission information. Eng Fail Anal 118:104899

Wang Z, Wang LZ, Li LL, Wang JC (2014) Failure mechanism of tunnel lining joints and bolts with uneven longitudinal ground settlement. Tunn Undergr Space Technol 40:300–308

White FM (2011) Fluid mechanics (Seventh Edition). McGraw-Hill

Wu HN, Shen SL, Liao SM, Yin ZY (2015) Longitudinal structural modelling of shield tunnels considering shearing dislocation between segmental rings. Tunn Undergr Space Technol 50:317–323

Wu HN, Shen SL, Yang J, Zhou AN (2018) Soil-tunnel interaction modelling for shield tunnels considering shearing dislocation in longitudinal joints. Tunn Undergr Space Technol 78:168–177

Wu MQ (2004) Application study on steel fiber concrete segment in metro tunnel engineering. Guangdong Build Mater 3:6–8 **(in Chinese)**

Xu G, He C, Lu D, Wang S (2019) The influence of longitudinal crack on mechanical behavior of shield tunnel lining in soft-hard composite strata. Thin-Walled Struct 144:106282

Xu L (2005) Study on the longitudinal settlement of shield tunnel in soft soil. Tongji University, Shanghai, China **(in Chinese)**

Ye G, Han L, Yadav SK, Bao X, Liao C (2020) Investigation on the tail brush induced loads upon segmental lining of a shield tunnel with small overburden. Tunn Undergr Space Technol 97:103283

Ye JN, Liu Y, Chen RP, Tang LJ (2014) Study of the permissible value of upward floating for segment in shield tunnel construction. Chin J Rock Mech Eng 33:4067–4074 **(in Chinese)**

You YF, Liang KS, Tan HL (2012) Optimization of mixing proportion of grout for simultaneous grouting in shield tunneling. Tunnel Constr 32:816–820

Youn BY, Breitenbücher R (2014) Influencing parameters of the grout mix on the properties of annular gap grouts in mechanized tunneling. Tunn Undergr Space Technol 43:290–299

Youn BY, Breitenbücher R (2018) Consolidation of single-component grouting mortars in the course of dewatering: redistribution of particles. Int J Civ Eng 17:33–43

Yu H (2011) The Optimization test research for the ratio of concrete back fill grouting the segment in shield tunneling. Beijing Jiaotong University, Beijing **(in Chinese)**

Zaheri M, Ranjbarnia M, Dias D, Oreste P (2020) Performance of segmental and shotcrete linings in shallow tunnels crossing a transverse strike-slip faulting. Transp Geotech 23:100333

Zhou J, Zhou S, Wu D, Zhu H (2013) Theory and experiment research on repair strength of damaged shield tunnel segment. Chin J Rock Mech Eng 32:3643–3649 **(in Chinese)**

Zhou SH, Ji C (2014) Tunnel segment uplift model of earth pressure balance shield in soft soils during subway tunnel construction. Int J Rail Transp 2:221–238

Publisher's Note Springer Nature remains neutral with regard to jurisdictional claims in published maps and institutional affiliations.